Fuel 195 (2017) 299–313

Contents lists available at ScienceDirect

Fuel

journal homepage: www.elsevier.com/locate/fuel

Full Length Article

Scaling analysis of the In-Situ Upgrading of heavy oil and oil shale

Julien Maes [a,*], Ann H. Muggeridge [b], Matthew D. Jackson [b], Michel Quintard [c], Alexandre Lapene [d]

[a] Institute of Petroleum Engineering, Heriot-Watt University, Edinburgh EH14 4AS, United Kingdom
[b] Department of Earth Sciences and Engineering, Imperial College London, South Kensington Campus, London SW7 2AZ, United Kingdom
[c] Université de Toulouse, INPT, UPS, Institut de Mécanique des Fluides de Toulouse, Allée Camille Soula, F-31400 Toulouse, France
[d] TOTAL E&P USA, 705 Forest avenue, Palo Alto, CA 94301, USA

ARTICLE INFO

Article history:
Received 23 November 2015
Received in revised form 17 January 2017
Accepted 19 January 2017
Available online 31 January 2017

Keywords:
In-Situ Upgrading
Heavy oil
Oil shale
Dimensionless numbers

ABSTRACT

The In-Situ Upgrading (ISU) of heavy oil and oil shale is investigated. We develop a mathematical model for the process and identify the full set of dimensionless numbers describing the model. We demonstrate that for a model with n_f fluid components (gas and oil), n_s solid components and k chemical reactions, the model was represented by $9 + k \times (3 + n_f + n_s - 2) + 8n_f + 2n_s$ dimensionless numbers. We calculated a range of values for each dimensionless numbers from a literature study. Then, we perform a sensitivity analysis using Design of Experiments (DOE) and Response Surface Methodology (RSM) to identify the primary parameters controlling the production time and energy efficiency of the process. The Damköhler numbers, quantifying the ratio of chemical reaction rate to heat conduction rate for each reaction, are found to be the most important parameters of the study. They depend mostly on the activation energy of the reactions and of the heaters temperature. The reduced reaction enthalpies are also important parameters and should be evaluated accurately. We show that for the two test cases considered in this paper, the Damköhler numbers needed to be at least 10 for the process to be efficient. We demonstrate the existence of an optimal heater temperature for the process and obtain a correlation that can be used to estimate it using the minimum of the Damköhler numbers of all reactions.

1. Introduction

Heavy oil and oil sands are important hydrocarbon resources that account for over 10 trillion barrels [1], nearly three times the volume of conventional oil in place in the world. Thermal EOR (Enhanced Oil Recovery) techniques are generally applied to very viscous heavy oil. In the Steam Assisted Gravity Drainage (SAGD) process, steam is injected from a well and forms a saturated zone. The steam flows to the perimeter of this vapour chamber from the wells and condenses. The heat is transferred by thermal conduction to the surrounding reservoir, the viscosity of the oil is reduced and so it flows, driven by gravity, to a horizontal production well below. SAGD was first introduced in the early 1980's by Butler and co-workers [2] and has been described and used in several pilots and commercial projects [3,4]. However, such a process comes with two main drawbacks; firstly, it require tremendous quantities of water, and secondly, the resulting hydrocarbons are still extra heavy oil/bitumen. Pipe transport of such viscous oil is challenging and refining on site is often required.

As an alternative, the process of In-Situ Upgrading (ISU) by subsurface pyrolysis has been applied in various pilot projects and laboratory experiments [5,6]. The idea behind ISU is to use subsurface electrical heaters to bring the formation to a high temperature of about 350 °C. At this temperature, the long chain hydrocarbon structures that mostly compose bitumen decompose through a series of chemical reactions of pyrolysis and cracking. Initially, this will occur in a zone near the heat source. As the heat propagates through the formation, initially by thermal conduction, a reaction zone propagates following the heat front. The pressure in the heated domain increases due to thermal expansion and creation of lighter products and the fluids flow toward the production well. This fluid transport also enables further heat transfer via convection. As the heat continue to propagate in the domain, more bitumen is converted and more hydrocarbons are produced.

During an ISU process, the undesirable products of the pyrolysis such as coke are left in the rock formation because the upgrading takes place in the reservoir. The main product of the upgrading is formed of molecules of lower molecular weight (typically lower than C30) that become volatile at modest temperatures. In addition, the viscosity of the oil phase is reduced by both the temperature and the conversion, unlike simple temperature-led

* Corresponding author.
E-mail address: julien.maes@pet.hw.ac.uk (J. Maes).

http://dx.doi.org/10.1016/j.fuel.2017.01.072
0016-2361/

Nomenclature

Variables

A	pre-exponential factor (s^{-1})
a	mass stoechiometric coefficient (no unit)
A_c	acentric factor (no unit)
C	mole concentration (mol/m^3)
c	compressibility (1/Pa)
D	depth (no unit)
E_a	activation energy (J/mol)
e	thermal expansion (1/K)
g	gravity constant (9.81 m/s^2)
h	specific enthalpy (J/kg)
K	absolute permeability (m^2)
L	domain length (m)
m_w	molecular weight (kg/mol)
P	pressure (Pa)
P_c	critical pressure (Pa)
R	universal gas constant (8.314 J/mol/K)
r	reaction rate ($kg/m^3/s$)
S	saturation (no unit)
T	temperature (K)
t	time (s)
T_c	critical temperature (K)
T_H	heater temperature (K)
u	specific energy (J/kg)
v	velocity (m/s)
α	permeability function parameter
Δh_r	reaction enthalpy (J/kg)
γ	specific heat capacity (J/kg/K)
κ	thermal conductivity (W/m/K)
μ	viscosity (Pa s)
ω	mass fraction (no unit)
ϕ	rock porosity (no unit)
ρ	mass density (kg/m^3)
τ	time scale of heat conduction in domain (s)

Subscript

0	initial value
g	gas phase
o	oil phase
r	inert rock
s	solid phase

viscosity reduction observed in standard SAGD processes [7]. As a result, the efficiency of the process, estimated by the Energy Return Over Investment (EROI) ratio, is potentially large compared to SAGD. Moreover, no water is used at the recovery stage, so using ISU can reduce costs by reducing the amount of infrastructure required on site for separation and treatment of the produced oil prior to transportation.

ISU can also be applied to oil shale reservoirs. Kerogen, the organic matter contained in oil shales is similar to the organic matter of source rocks that transform to petroleum fluids through geological time [8]. In oil shales, the natural maturation process, which would eventually lead to oil and gas, is at a very early stage and may still require millions of years and deeper burial. This process can be accelerated through ISU [9]. The initial decomposition of kerogen gives an asphaltene-rich heavy oil which then pyrolyses further in a manner very similar to heavy oil upgrading. The main differences between heavy oil and oil shale upgrading are that (1) the primary reactant for oil shales is solid rather than very viscous liquid and (2) unlike oil sands, oil shales initially have a very low permeability. During the initial stages of pyrolysis the reaction products are trapped in pores within the solid, resulting in an increase of pressure in the heated domain. However, as more of the solid decomposes, these pores become interconnected and the liquid and/or gas can flow away from the reaction zone and to the producer well.

The ISU process generally uses horizontal [10] or tightly spaced vertical electrical heaters [5] to slowly and uniformly heat the formation by thermal conduction to the conversion temperature. Fig. 1 shows the well pattern for the Mahogany Field Experiment, which is a part of Shell's Colorado field pilot [5]. For these experiments, the distance between two wells varied from 2 ft ($\simeq$ 0.6 m) to 30 ft ($\simeq$ 9 m).

Thermal cracking of extra-heavy oil and oil shale can be described by a compositional kinetic model. One such model for oil shale pyrolysis was developed by Braun and Burnham [11] for oil shale pyrolysis. It contains 83 species and 100 reactions. Fan et al. [12] present an adapted kinetic model that includes three hydrocarbon components and five chemical reactions. For this, they modified the previous model to eliminate water and prechar, and they performed a component-lumping process to map the hydrocarbon species to three lumped pseudo-components. For

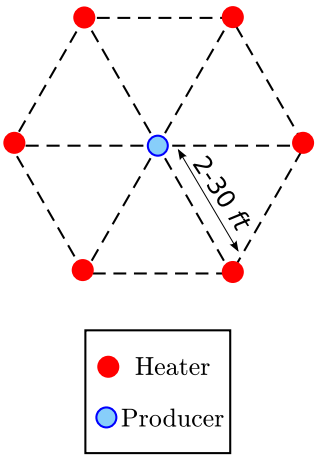

Fig. 1. Top view of well pattern for the in situ upgrading process, Mahogany field experiment (figure from [5]).

bitumen pyrolysis, Behar et al. [13] developed a kinetic model that contains 11 lumped chemical classes and 32 reactions.

The outcome of the ISU process depends on a large number of physical parameters, the values of which are usually uncertain. For example, the calibration of kinetic models from laboratory to reservoir condition is often challenging [13]. Scaling using dimensionless numbers can provide useful insight into the relative importance of different parameters and physical processes. Design of Experiment (DOE) [14] allows quantification of the impact of the dimensionless parameters with a minimal amount of computation. Dimensionless numbers are often used to scale laboratory results to the application length scale and conditions, and may be developed using techniques such as Dimensional Analysis (DA) [15] and Inspectional Analysis (IA) [16]. Ranking the different parameters controlling a given thermal decomposition application enables experimental programs to be focused on acquiring the relevant data with the appropriate accuracy.

This paper has four objectives: (1) to present a set of dimensionless numbers that describes the ISU process, (2) to demonstrate the importance of using accurate activation energies, (3) to

demonstrate the importance of including reaction enthalpies in the model and (4) to study the impact of heater temperature on the production time and energy efficiency of the process and demonstrate the existence of an optimal heater temperature.

This paper is organised in five parts. Firstly, we extend the mathematical model presented by Maes et al. [17] for simulation of ISU of bitumen so that it can be used to simulate ISU of both bitumen and oil shale. This model has been previously validated by comparison with experimental data presented in Kumar et al. [6]. Secondly, we present two test cases. Test case 1 describes the ISU of Athabasca bitumen, and test case 2 describes the ISU of Green River oil shale. Test case 2 uses a kinetic model with uncharacteristically low activation energy and pre-exponential factor for the decomposition of kerogen. Thirdly, we identify the set of dimensionless groups that fully described the model and compute for each of them the value for test cases 1 and 2, as well as a range of values computed from a literature study. We explore the impact of the uncharacteristically low activation energy and pre-exponential factor on the Damköhler number, which describes the ratio of chemical reaction to heat diffusion at the heater temperature. We also compute reduced reaction enthalpies, which describe the ratio of heat consumed by chemical reactions to heat stored in the reactants for the values of reaction enthalpies published in the literature [18,19]. Fourthly, we perform a sensitivity analysis using Design of Experiment (DOE) [14] on a simplified model with one reaction to identify the primary parameters controlling the production time and energy efficiency of the process. We observe that the Damköhler number and the reduced reaction enthalpy are both primary numbers. Finally, we return to test cases 1 and 2 and study the impact of the Damköhler numbers and the reduced reaction enthalpies on the production profiles. We demonstrate the importance of using accurate activation energies and reaction enthalpies, and show the existence of an optimal heater temperature for the energy efficiency of the process.

2. Mathematical model

The model contains an inert rock (r), with the pore-space occupied by n hydrocarbon components regrouped into three phases: gas (g), liquid (l) and solid (s). The solid phase is formed of kerogen and/or coke. We assume that the model contains k thermally unstable chemical entities which decompose with first-order kinetics. The decomposition of an entity X_i, $i = 1 \dots k$, can be accounted for by one chemical reaction with one reactant:

$$X_i \xrightarrow{r_i} a_{i,1}X_1 + \cdots + a_{i,h}X_h + \cdots + a_{i,n}X_n \tag{1}$$

where r_i is the rate of reaction i and $a_{i,j}$ the mass stoichiometric coefficient for product j ($a_{i,j} > 0$). The rate of reaction is described using an Arrhenius law of order 1 [20]:

$$r_i = A_i \exp\left(-\frac{E_{ai}}{RT}\right) C_i \tag{2}$$

where A_i and E_{ai} are the frequency factor and the activation energy of reaction i, R is the universal gas constant and C_i is the mass concentration of the reactant X_i of reaction i.

The mass-balance equation for compositional simulation for each hydrocarbon component $j = 1 \dots n$ can be expressed as follows [21]:

$$\frac{\partial}{\partial t}\left(\phi \sum_p \omega_{p,j}\rho_p S_p\right) = -\nabla\left(\sum_p \omega_{p,j}\rho_p v_p\right) + \sum_i a_{i,j} r_i \tag{3}$$

where ϕ is the inert rock porosity, S_p, ρ_p and v_p the saturation, mass density and velocity of phase p, $\omega_{p,j}$ the mass fraction of component j in phase p. The porosity of the inert rock change with pressure due to compressibility:

$$\phi = \phi_0(1 + c_r(P - P_0)) \tag{4}$$

where ϕ_0 is the initial inert rock porosity and c_r is the inert rock (pore volume) compressibility. The density of the gas phase is given by the ideal gas law:

$$\rho_g = \frac{m_{wg}P}{RT} \tag{5}$$

where m_{wg} is the total gas molecular weight:

$$m_{wg} = \sum_j \omega_{g,j} m_{wj} \tag{6}$$

The density of the liquid phase is given by:

$$\begin{aligned} \frac{1}{\rho_o} &= \sum_j \frac{\omega_{o,j}}{\rho_{o,j}} \\ \rho_{o,j} &= \frac{\rho_{o,j,0}}{(1 - c_j(P - P_0))(1 + e_j(T - T_0))} \end{aligned} \tag{7}$$

where $\rho_{o,j,0}, c_j$ and e_j are the component initial density, compressibility and thermal expansion in the liquid phase, respectively. We neglect the solid phase compressibility and thermal expansion, so that the solid density only depends on the phase composition:

$$\frac{1}{\rho_s} = \sum_j \frac{\omega_{s,j}}{\rho_{s,j}} \tag{8}$$

where $\rho_{s,j}$ is the component density in the solid phase. The velocity of phase p is given by Darcy's law:

$$v_p = -K\frac{k_{rp}}{\mu_p}\nabla\left(P - \rho_p g D\right) \tag{9}$$

where P is the pressure, g the gravitational constant, D the depth, K the absolute permeability and $k_{r,p}$ and μ_p are the relative permeability and viscosity of phase p. The solid phase is immobile ($k_{rs} = 0$). The gas-oil relative permeability is described by a Corey-type correlation [22] with a critical gas saturation of $S_{gc} = 0.05$, a residual oil saturation of $S_{or} = 0.2$ and Corey exponents equal to 2 for both oil and gas phases.

$$\begin{aligned} k_{ro} &= \left(\frac{S_o - S_{or}}{1 - S_{or} - S_{gc}}\right)^2 \\ k_{rg} &= \left(\frac{S_g - S_{gc}}{1 - S_{or} - S_{gc}}\right)^2 \end{aligned} \tag{10}$$

In this work, we do not study the effect of changing the relative permeability curves so S_{gc} and S_{or} are constant for the rest of the study.

To describe the effect of kerogen decomposition and/or coke formation in the pore space, we use the concept of an Evolving Porosity Medium (EPM) [23]. The apparent porosity is defined as $\phi(1 - S_s)$, where S_s is the solid saturation ($S_s = 1 - S_g - S_o$). The impact of the solid saturation on the absolute permeability is given by a simple exponential relationship:

$$K = K_0 \exp\left(-\alpha(S_s - S_{s,0})\right) \tag{11}$$

where K_0 is the initial permeability. The coefficient α determines how strongly the absolute permeability varies with a change in solid saturation. Typically, α has a value between 5 and 20 [24]. Phase equilibrium is modelled using Wilson K-values [25]:

$$\begin{aligned} \xi_{g,j} &= K_j(P,T)\xi_{o,j} \\ K_j(P,T) &= \exp\left(\Omega_j\right)\frac{P_{cj}}{P} \\ \Omega_j &= d_w(1 + A_{cj})\left(1 - \frac{T_{cj}}{T}\right) \end{aligned} \tag{12}$$

where $\xi_{p,j}$ is the molar fraction of component j in phase p, A_{cj}, P_{cj} and T_{cj} are the component acentric factor, critical pressure and critical temperature, respectively, and $d_w = 5.373$ is Wilson's constant. The molar fractions can be computed from the mass fractions using:

$$\xi_{p,j} = \frac{\omega_{p,j}/m_{wj}}{\sum_l \omega_{p,l}/m_{wl}} \tag{13}$$

Heat transfer is accounted for in the overall energy balance equation [26]:

$$\frac{\partial}{\partial t}\left((1-\phi)\rho_r u_r + \phi\sum_p \rho_p u_p S_p\right) = \nabla(\kappa\nabla T) - \nabla\left(\sum_p \rho_p v_p h_p\right) + \sum_i \Delta h_{ri} r_i \tag{14}$$

where ρ_r and u_r are the inert rock density and internal energy, u_p and h_p are the phase internal energy and enthalpy, κ is the thermal conductivity of the system and Δh_{ri} is the enthalpy of reaction i.

Our numerical model include three major approximations. Firstly, experimental correlations for phase equilibrium and phase properties are used instead of more accurate equations of state. Secondly, water has not been included, since in ISU, the reactions of interest occur mostly above the boiling point of water. Finally, heat loss has been neglected in Eq. (14). Fan et al. [12] demonstrated that heat loss to overburden and underburden could have an impact on the efficiency of the process depending on the ratio of formation thickness to well spacing. The wider the well spacing and the thinner the formation then the more important heat loss becomes. Here we chose to neglect it to focus on the other mechanisms of the process.

3. Test cases

In this paper, we considered two test cases, one describing the ISU of Athabasca tar-sand (test case 1), and one representing the ISU of Green River oil shale (test case 2). These test cases are similar in the sense that they describe the decomposition of one primary reactant (bitumen compound NSO for test case 1 and kerogen K for test case 2) into heavy, medium and light hydrocarbon components and solid residue PrC, with secondary decomposition for the heavy and medium components. Apart from different values for the reaction parameters, the main difference is in the initial phase saturations. For tar-sand, the pore-space is initially 90% filled with very viscous liquid oil (NSO) and 10% with gas (H_2S-CO_2). The absolute permeability is high but the initial viscosity of the liquid phase is very large, so initially the fluid is almost immobile. However, when the temperature increases, the viscosity decreases rapidly leading to a small oil production rate. For oil shale, the pore-space is initially 85% filled at with a solid phase (kerogen) and 15% with gas CO_2 and remains like this until the chemical reactions become important. There is no initial oil production. The initial permeability is very low and most of the hydrocarbon is immobile. Therefore, these two test cases have similar kinetic models but very different flow behaviour.

For both test cases, we consider a 3D reservoir represented by a cube of length $L = 10$ m and we consider a simplified heater pattern formed by four heaters, one on each vertical side of the cube, and one producer well in the centre (Fig. 2). The heaters operate at a constant temperature $T_H = 350\,^\circ$C and the producer at a constant bottom hole pressure (bhp) equal to the initial pressure of the reservoir.

All numerical simulations are performed using a C++ code developed as part of the study for the modelling of ISU. We use the finite volume method with an $11 \times 11 \times 1$ grid with a fully implicit formulation and Newton's algorithm for the treatment of non-linearities [27].

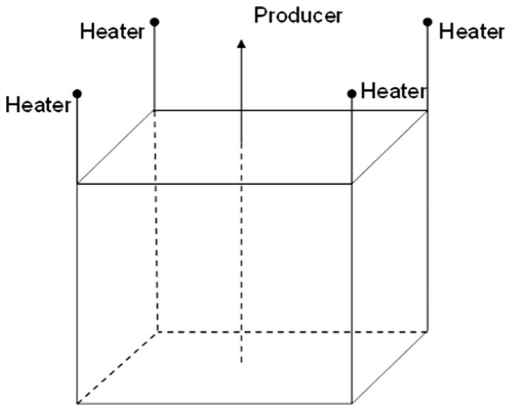

Fig. 2. Reservoir geometries and wells.

3.1. Test case 1: Athabasca bitumen

For this case, the pore space is initially filled with very viscous bitumen. The rock and initial properties are summarised in Table 1. The thermal conductivity is the value for the whole domain which includes inert rock, solid organic saturation and fluid saturations. Strictly, it depends on temperature and pore space composition, but we assume it constant to focus on other aspects. Rock heat capacity is also assumed constant. The porosity and permeability are high (0.36 and 4158 mD respectively) but the initial viscosity of the liquid phase is also large (150,000 cp). As the temperature increases inside the reservoir, the viscosity of the oil decreases following the correlation [28]:

$$\ln(\ln \mu_o) = -3.5912 \ln T + 22.976 \tag{15}$$

where μ_o is the oil viscosity in centipoise (cp). For the viscosity of the gas, we use the same simple correlation as the one used in CMG STARS [29]:

$$\mu_g = 0.0136 + 3.8 \times 10^{-5}(T - 273.15) \tag{16}$$

where μ_g is in cp, and T is in K. The bitumen decomposition is modelled using a kinetic scheme adapted from Behar et al. [13] and Al Darouich et al. [30]. This model uses the C14+ extracted from the Safaniya crude oil (Saudi Arabia). The reactions and components are lumped into a model with $k = 3$ reactions and $n = 6$ components (Table 2). The reaction enthalpies have been neglected here. Note that the activation energy of the C_{14+} component is larger than the ones that are common for most type of organic matter [31–33]. This is because Behar et al. [13] includes more stable structure of C_{14+} to match experiments at temperature larger than 350 °C. The

Table 1
Rock and initial properties for test case 1. These data are adapted from [6].

	Test case 1
Initial porosity	0.36
Initial permeability	4158 mD
Coefficient α	6.28
Initial reactant saturation	0.9
Rock heat capacity	1800 kJ/m^3/K
Heat conductivity	1.7 W/(m K)
Rock compressibility	5×10^{-3} 1/MPa
Initial pressure	1.5 MPa
Initial temperature	28 °C

Table 2
Chemical reactions for test case 1. These data are adapted from [13].

Reactional reactions for test	A (s^{-1})	E_a (kJ/mol)	Δh_r[†] (kJ/kg)
NSO ⟶ 0.170 C_{14+} + 0.105 C_{6-13} + 0.079 C_{1-4} + 0.051 H_2S-CO_2 + 0.595 PrC	7.82×10^{12}	209.2	0
C_{14+} ⟶ 0.48 C_{6-13} + 0.248 C_{1-4} + 0.272 PrC	3.85×10^{16}	259.4	0
C_{6-13} ⟶ 0.767 C_{1-4} + 0.233 PrC	3.85×10^{16}	276.1	0

[†] Initially reaction enthalpies are neglected.

thermodynamic properties of the components are summarised in Table 3.

3.2. Test case 2: Green River oil shale

For this case, the pore space is initially filled with solid kerogen ($S_s = 0.85$) and CO_2 gas ($S_g = 0.15$). The rock properties are summarised in Table 4. Thermal conductivity and rock heat capacity are assumed constant. The rock porosity is equal to 0.2 but as the solid is immobile, the apparent porosity for the fluid is equal to $0.2 \times (1 - 0.85) = 0.03$. The initial permeability of the domain (inert rock filled with kerogen) is also very low (2 μD). The viscosity of the gas is given by Eq. (16) and the viscosity of the liquid phase is given by [34]:

$$\log_{10}\mu_o(T) = \frac{4.1228}{\left(1 + \frac{T-303.15}{303.15}\right)^{3.564}} - 0.002 \tag{17}$$

where μ_o is in cp and T in K. As the temperature increases, the kerogen decomposes into liquid and gas products. The solid saturation decreases and the apparent porosity $\phi(1 - S_s)$ increases. The permeability in the domain also increases following Eq. (11). We used a simplified kinetic model adapted from Wellington et al. [35] and described in Fan et al. [12]. This model includes $k = 3$ reactions and $n = 6$ components. Note that the activation energy and the pre-exponential factor for the decomposition of kerogen presented in Table 5 are small compared to the one commonly used for describing cracking of kerogen [11,32]. The thermodynamic properties of the components are summarised in Table 6.

4. Dimensionless analysis

We used Inspectional Analysis to identify the dimensionless numbers describing our mathematical model. This method has been previously used to analyse various processes including immiscible water flooding [16], miscible displacement in heterogeneous permeable media [36] and heat and mass flow in the presence of pyrolysis [37]. The underlying physical laws, expressed in the form of partial differential equations and boundary conditions are analysed to determine the minimum set

Table 4
Rock and initial properties for test case 2. These data are adapted from [12,24].

	Test case 1
Initial porosity	0.2
Initial permeability	2 μD
Coefficient α	6.28
Initial solid saturation	0.85
Rock heat capacity	1800 kJ/m^3/K
Heat conductivity	2 W/(m K)
Rock compressibility	4.35×10^{-4} 1/MPa
Initial pressure	0.69 MPa
Initial temperature	16.7 °C

Table 5
Chemical reactions for test case 2. These data are adapted from [12].

Reaction	A (s^{-1})	E_a (kJ/mol)	Δh_r[‡] (kJ/kg)
K ⟶ 0.280 IC_{37} + 0.200 IC_{13} + 0.090 IC_2 + 0.015 CO_2 + 0.415 PrC	4.33×10^{7}	161.6	0
IC_{37} ⟶ 0.090 IC_{13} + 0.170 IC_2 + 0.740 PrC	7.23×10^{11}	206.0	0
IC_{13} ⟶ 0.200 IC_2 + 0.800 PrC	1.14×10^{12}	219.3	0

[‡] Initially reaction enthalpies are neglected.

of dimensionless groups required to describe the problem. An important step is the identification of a reference time scale for the process. In the case of ISU, there are several time scales that could be used, such as the time scale of heat conduction, or the various time scales of the chemical reactions. Since the pore space is initially filled with solid or very viscous liquid, convection is limited. Heat conduction is then the primary mechanism for heat propagation in the domain, which induces the chemical reaction. Therefore, we chose the time scale of heat conduction in the rock as our reference time scale:

$$\tau = \frac{(1-\phi)\rho_r\gamma_r L^2}{\kappa} \tag{18}$$

This time is equal to 785 and 833 days for test cases 1 and 2, respectively. Following the methodology described by Shook [16], we obtained the full set of dimensionless numbers representing the system. For clarity, they are regrouped into three categories: the general heat and mass flow numbers, the chemical reaction numbers and the numbers that described component properties.

4.1. Dimensionless numbers

Table 7 shows the numbers describing the heat and mass flow. In the absence of injection, the convection is not described by the Péclet number, equal to the ratio of injected fluid rate to heat conduction rate, but instead by the pressure Lewis number L_e, which quantifies the ratio of heat diffusivity to pressure diffusivity in

Table 3
Component thermodynamic properties for test case 1.

	NSO	C_{14+}	C_{6-13}	C_{1-4}	H_2S-CO_2	PrC
Molecular weight (kg/kmol)	515	500	160.0	40	80	12.72
Critical pressure (MPa)	0.6	0.6	2.1	4.2	4.0	NA
Critical temperature (K)	1200	950	670	370	350	NA
Acentric factor (no unit)	1.6	1.5	0.53	0.151	0.1	NA
Liquid density at standard condition (kg/m^3)	1070	940	800	400	400	NA
Liquid compressibility (1/MPa × 10^{-3})	5.4	5.4	5.4	5.4	5.4	NA
Liquid thermal expansion (1/K × 10^{-4})	6.3	6.3	6.3	6.3	6.3	NA
Solid density (kg/m^3)	NA	NA	NA	NA	NA	1200
Specific heat capacity (kJ/kg/K)	1.5	1.5	2.0	2.5	2.5	1.0
Initial mass composition	0.57	0.41	0.02	0	0	0

Table 6
Component thermodynamic properties for test case 2.

	IC_{37}	IC_{13}	IC_2	CO_2	K	PrC
Molecular weight (kg/kmol)	465.83	169.52	30.07	44.01	15	12.72
Critical pressure (MPa)	0.94	2.4	4.6	7.4	NA	NA
Critical temperature (K)	962.28	715.36	288.74	298.53	NA	NA
Acentric factor (no unit)	0.818	0.365	0.008	0.239	NA	NA
Liquid density at standard condition (kg/m^3)	1013	760	400	400	NA	NA
Liquid compressibility ($1/MPa \times 10^{-3}$)	5.4	5.4	5.4	5.4	NA	NA
Liquid thermal expansion ($1/K \times 10^{-4}$)	6.3	6.3	6.3	6.3	NA	NA
Solid density (kg/m^3)	NA	NA	NA	NA	1200	1200
Specific heat capacity (kJ/kg/K)	1.5	2.0	2.5	2.5	1.0	1.0
Initial mass composition	0	0	0	0.001	0.999	0

Table 7
General heat and mass flow scaling groups for ISU.

Name	Notation	Definition
Pressure Lewis number	L_e	$\frac{\phi_0 \mu_{g0} L^2}{K_0 P_0 \tau}$
Oil gas viscosity ratio	M	$\frac{\mu_o}{\mu_g}$
Heat capacity ratio	Γ	$\frac{\phi_0 \rho_{R0} \gamma_R}{(1-\phi_0)\rho_r \gamma_r}$
Reduced initial temperature	T_0^*	$\frac{T_0}{T_H - T_0}$
Initial saturation of reactant	$S_{R,0}$	
Permeability function parameter	α	
Reduced gas viscosity derivative	$\delta\mu_g^*$	$\frac{d\mu_g}{dT}\frac{T_H - T_0}{\mu_{g,0}}$
Reduced rock compressibility	c_r^*	$c_r P_0$

the gas phase. The ratio of heat diffusivity to pressure diffusivity in the oil phase is described by the quantity $M \times L_e$, where M is the oil gas viscosity ratio. Since M varies with temperature, we define M_0 as the initial viscosity ratio and M_H as the viscosity ratio at heater temperature. The larger L_e and $M \times L_e$ are, the higher the pressure rises during the process. The heat capacity ratio Γ represents the ratio between the heat capacity of the primary reactant in the pore space and the heat capacity of the inert rock. The larger Γ is, the more energy is required to heat up the domain and the less efficient is the process. The other dimensionless numbers are the reduced initial temperature T_0^*, the initial saturation of reactant $S_{R,0}$, the permeability function parameter α, the reduced gas viscosity derivative $\delta\mu_g^*$ and the reduced inert rock pore volume compressibility c_r^*. Table 8 gives the values of these numbers for test cases 1 and 2.

We observe that test case 1 has a Lewis number three order of magnitude smaller than test case 2. This can be explained by the difference in the initial permeability of the Athabasca bitumen reservoir and the Green River oil shale reservoir. This indicates that the mechanical stress due to the pressure rise during an ISU process for an oil shale reservoir can be very large and potentially lead to the formation of fractures [38]. In this work, we ignore fractures and assume that the permeability of the rock always follows Eq. (11).

Table 8
Values of general heat and mass flow scaling groups for test cases 1 and 2.

	Test case 1	Test case 2
L_e	1.3×10^{-6}	2.9
Γ	0.5	0.17
M_0	10^7	4.8×10^6
M_H	89	77
T_0^*	0.94	0.87
$S_{R,0}$	0.9	0.85
α	6.28	6.28
$\delta\mu_g^*$	0.83	0.89
c_r^*	7.5×10^{-3}	3×10^{-4}

Each reaction $i = 1 \ldots k$ is described by three dimensionless numbers: the Damköhler number D_{Ki}, the Arrhenius number N_{ai} and the reduced reaction enthalpy Δh_{ri}^*, plus n stoichiometric coefficients (Table 9). The Damköhler number D_{Ki} quantifies the ratio of chemical reaction rate to heat conduction rate at the heater temperature. For each reaction, the Arrhenius numbers N_{ai} describes the energy barrier to the reaction and the reduced reaction enthalpy Δh_{ri}^* quantifies the ratio of heat consumed by that chemical reaction to heat stored in the reactant. Table 10 gives the values of these numbers for test cases 1 and 2.

We observe that for test case 1, the lighter the reactant, the larger the Damköhler number. However, for test case 2, the Damköhler number for the decomposition of kerogen (reaction 1) is smaller than the Damköhler number for the decomposition of heavy oil (reaction 2). This surprising result comes from the fact that the activation energy and the pre-exponential factor for the decomposition of kerogen presented in Table 5 are small compared to the one commonly used for describing cracking of kerogen [11,32].

The Damköhler number depends mostly on the activation energy and on the heater temperature. Indeed, a change of 1% for the values of the pre-exponential factor changes the Damköhler number by 1%, but an increase of 1% of the activation energy for the kerogen decomposition (test case 2, reaction 1) decreases the Damköhler number by 27%. This shows that, to model accurately the chemical reactions over a wide range of temperature, the activation energies must be measured accurately.

In Wellington et al. [35], the kinetic models are given with activation energies and pressure-dependent pre-exponential factors that have been experimentally determined over a temperature range from 0 to 300 °C. On the contrary, Braun and Burnham [31] proposed several kerogen decomposition models that have been experimentally validated over a wider range of temperature, from 0 to 600 °C. For these models, the pre-exponential factor $A = 3 \times 10^{13}$ is much larger than $A = 4.33 \times 10^7$ defined by Wellington et al. [35], and the activation energies range from 49 kcal/mol (= 205.016 kJ/mol) to 53 kcal/mol (= 221.752 kJ/mol), which is also much larger than $E_a = 161.6$ kJ/mol defined by Wellington et al. [35]. For this range of activation energies, the Damköhler number ranges from 500 to 14,000. So the Damköhler number for the decomposition of kerogen obtained using the Wellington et al. kinetic model is wrong by a factor of between 5 and 150.

Table 9
Chemical reaction scaling groups for each reaction $i = 1..k$.

Name	Notation	Definition
Damköhler number	D_{Ki}	$A_i \exp\left(\frac{E_{ai}}{RT_H}\right)\tau$
Arrhenius number	N_{ai}	$\frac{E_{ai}}{R(T_H - T_0)}$
Reduced reaction enthalpy	Δh_{ri}^*	$-\frac{\Delta h_{Ri}}{\gamma_R (T_H - T_0)}$

Table 10
Values of chemical reaction scaling groups for test cases 1 and 2.

	Test case 1			Test case 2		
Reac.	1	2	3	1	2	3
D_{Ki}	1540	470	19	90	280	34.0
N_{ai}	78.1	96.9	103	58.3	74.3	79.1
Δh^*_{ri}	0	0	0	0	0	0

We conclude that the model defined in Table 5 underestimates the Damköhler number for the decomposition of kerogen. The sensitivity analysis conducted in the next section will show that the Damköhler numbers are the most important numbers controlling the energy efficiency of the process, so evaluating them accurately is essential. Later, we will explore the impact of getting the Damköhler numbers wrong by a factor of 100.

The reaction enthalpies are generally ignored in previous work describing numerical simulation of the ISU process [12,39,23]. In this paper, we initially neglect them, so that $\Delta h_{ri} = 0$ for all reaction. Phillips et al. [18] measured the enthalpies of pyrolysis of Athabasca bitumen in a nitrogen atmosphere. The reaction enthalpies of oil sand were found to be similar to the reaction enthalpies of oil shale obtained by Wen and Yen [40].

Table 11 shows the values measured and the corresponding reduced reaction enthalpies. These reduced reaction enthalpies ranges from 0.1 to 2.5. The sensitivity analysis conducted in the next section will demonstrate that they can have an important impact on the production time and the energy efficiency of the process.

Finally, for each component $j = 1 \ldots n$, the thermodynamic properties are described by eight dimensionless numbers for liquid and gas components and two for solid components. They are presented in Tables 12 and 13, and their values for test cases 1 and 2 are given in Tables 14 and 15, respectively. For Athabasca bitumen, the primary reactant $R = NSO$. For Green River oil shale, $R = K$.

4.2. Range of values for the dimensionless numbers

To establish the range of values for the dimensionless numbers, we first need to establish the range of values for the various parameters of the ISU process. These have been selected from a thorough literature review. For the rock and initial properties, we used papers describing the numerical simulation of oil shale or bitumen recovery processes [12,24,6,41]. For the chemical reaction properties, we reviewed Braun et al. [11], Behar et al. [13] and Phillips et al. [18]. Finally, we used Perry's Handbook [42] for the thermodynamic properties of the components. Table 16 shows the range obtained for each parameter.

In reality, data for component or chemical reaction properties are not independent, but here they are assumed to be in order to define the range of dimensionless groups. Dependencies between parameters should be explored in future work as this may reduce the set of primary numbers obtained from the analysis. Assuming they are independent, we obtain a range of values for each dimensionless group. They are given in Table 17.

The Damköhler numbers and the pressure Lewis number are the numbers that vary the most, over a range of five and nine orders of magnitude, respectively. For small $D_{Ki} \approx 0.04$, the chemical reaction is very slow everywhere in the reservoir, which suggests that the heater temperature is too small. For large $D_{Ki} \approx 2.0 \times 10^4$, the reaction is very fast when the temperature gets near the heater temperature, which suggests that T_H could have been set to a lower value. For the pressure Lewis number, small values $L_e \approx 1.4 \times 10^{-8}$ correspond to domains with a large initial porosity (tar-sand) and large values $L_e \approx 45$ correspond to domains with a low initial porosity (oil shale).

The reduced gas density and the initial viscosity ratio vary over a range of three orders of magnitude. For the gas density, this shows the variability of the gas molar weight from the lightest components to the heaviest components that exist in the gas phase. For the initial viscosity ratio, the largest values correspond to extra-heavy oil (bitumen) and the lowest values correspond to heavy oil.

The heat capacity ratio Γ and the reduced rock compressibility c^*_r vary over a range of two order of magnitude. Large values correspond to highly porous highly compressible tar-sands while low values correspond to oil shale.

Finally, the reduced reaction enthalpy varies from 0 to 4. Low values describe the decomposition of kerogen and heavy components in general, while large values correspond to the decomposition of lighter oil components.

In the next section, the various ranges defined in Table 17 are used to perform a sensitivity analysis.

Table 12
Thermodynamic properties scaling groups for each fluid component $j = 1..n_f$.

Name	Notation	Definition
Reduced gas density	$\rho^*_{g,j}$	$\frac{m_{wj}P_0}{RT_0\rho_{R,0}}$
Reduced oil density	$\rho^*_{o,j}$	$\frac{\rho_{o,j}}{\rho_{R,0}}$
Reduced oil compressibility	c^*_j	$c_j P_0$
Reduced oil thermal expansion	e^*_j	$e_j(T_H - T_0)$
Acentric factor	A_{cj}	
Reduced critical pressure	P^*_{cj}	$\frac{P_{cj}}{P_0}$
Reduced critical temperature	T^*_{cj}	$\frac{T_{cj}}{T_0}$
Reduced specific heat capacity	γ^*_j	$\frac{\gamma_j}{\gamma_R}$

Table 13
Thermodynamic properties scaling groups for each solid component $j = 1..n_s$.

Name	Notation	Definition
Reduced solid density	$\rho^*_{s,j}$	$\frac{\rho_{s,j}}{\rho_{R,0}}$
Reduced specific heat capacity	γ^*_j	$\frac{\gamma_j}{\gamma_R}$

Table 11
Values of reaction enthalpies measured in Phillips et al. [18] and corresponding reduced reaction enthalpies.

	Test case 1			Test case 2		
Reac.	1	2	3	1	2	3
Δh_r (kJ/kg)	271	169	821	32	169	821
Δh^*_{ri}	0.56	0.31	1.7	0.1	0.51	2.5

Table 14
Values of thermodynamic properties scaling groups for each component for test case 1.

	NSO	C_{14+}	C_{6-13}	C_{1-4}	H_2S-CO_2	PrC
$\rho^*_{g,j}$	0.29	0.28	0.09	0.02	0.04	NA
$\rho^*_{o,j}$	1	0.88	0.75	0.37	0.37	NA
c^*_j	0.008	0.008	0.008	0.008	0.008	NA
e^*_j	0.20	0.20	0.20	0.20	0.20	NA
$\rho^*_{s,j}$	NA	NA	NA	NA	NA	1.12
γ^*_j	1	1	1.33	1.67	1.67	0.67
A_{cj}	1.6	1.5	0.53	0.151	0.1	NA
P^*_{cj}	0.4	0.4	1.4	2.8	2.67	NA
T^*_{cj}	3.98	3.15	2.22	1.23	1.16	NA

Table 15
Values of thermodynamic properties scaling groups for each component for test case 2.

	IC_{37}	IC_{13}	IC_2	CO_2	K	PrC
$\rho^*_{g,j}$	0.111	0.040	0.007	0.011	NA	NA
$\rho^*_{o,j}$	0.84	0.63	0.33	0.33	NA	NA
c^*_j	0.004	0.004	0.004	0.004	NA	NA
e^*_j	0.21	0.21	0.21	0.21	NA	NA
$\rho^*_{s,j}$	NA	NA	NA	NA	1	1
γ^*_j	1.5	2	2.5	2.5	1	1
A_{cj}	0.818	0.365	0.008	0.239	NA	NA
P^*_{cj}	1.36	3.48	6.67	10.7	NA	NA
T^*_{cj}	3.32	2.47	1.0	1.03	NA	NA

Table 16
Range of values for the various parameters of the ISU process. They are obtained from a thorough literature review [12,24,6,41,11,13,18,19,42].

Property	Min	Max	Property	Min	Max
L (m)	10	15	ϕ	0.1	0.4
K_0 (mD)	10^{-3}	5000	α	5	10
ρ_l (kg/m^3)	2000	2200	γ_l (J/(kg K))	900	1500
m_{wg} (kg/mol)	0.03	0.3	m_{wo} (kg/mol)	0.1	0.515
κ_s (W/(m K))	1	3	$S_{R,0}$	0.8	0.9
$r_i(T_H)$ (s^{-1})	10^{-9}	3×10^{-5}	E_{ai} (J/mol)	1.60×10^{5}	2.8×10^{5}
Δh_{ri} (J/kg)	0	1×10^{6}	a_{ij}	0	0.8
ρ_R (kg/m^3)	1000	1500	γ_R (J/(kg K))	1000	1500
$\rho_{o,j}$ (kg/m^3)	400	1070	$\rho_{s,j}$ (kg/m^3)	1000	1500
c_j (1/Pa)	10^{-9}	6×10^{-9}	e_j (1/K)	4×10^{-4}	10^{-3}
γ_j (J/(kg K))	1000	2500	A_{cj}	0.008	1.6
P_{cj} (Pa)	6×10^{5}	8×10^{6}	T_{cj} (K)	280	1200
$\mu_{g,0}$ (Pa s)	1×10^{-5}	2×10^{-5}	$\delta\mu_g$ (Pa s/K)	2×10^{-8}	4×10^{-8}
$\mu_{o,0}$ (Pa s)	10	1000	$\mu_{o,H}$ (Pa s)	2×10^{-3}	3×10^{-3}
T_H (°C)	300	400	T_0 (°C)	10	40
P_0 (Pa)	5×10^{5}	5×10^{6}	c_r ($1/P_a$)	4×10^{-10}	5×10^{-9}

Table 17
Range of values for the dimensionless numbers of the ISU process. They are obtained by combining minimum and maximum values of dimensional parameters given in Table 16.

Group	Min	Max	Group	Min	Max
L_e	1.4×10^{-8}	45	Γ	0.03	0.83
M_0	5×10^{5}	1×10^{8}	M_H	67	197
T^*_0	0.73	1.2	$S_{R,0}$	0.8	0.9
$\delta\mu^*_g$	0.26	1.56	α	5	10
c_r	2×10^{-4}	2.5×10^{-2}	D_{Ki}	0.04	2.0×10^{4}
N_{ai}	50	130	Δh^*_{ri}	0	4.0
a_{ij}	0	0.8	$\rho^*_{g,j}$	4×10^{-3}	0.64
$\rho^*_{o,j}$	0.27	1.1	c^*_j	5×10^{-4}	0.03
e^*_j	0.1	0.4	$\rho^*_{s,j}$	0.67	1.5
γ^*_j	0.67	2.5	A_c	0.008	1.6
P^*_c	0.12	16	T^*_{cj}	0.89	4.2

5. Sensitivity analysis with DOE

In order to identify the most important parameters for the production time and the energy efficiency of the process, we perform a sensitivity analysis using DOE. The number of dimensionless groups increases rapidly with the numbers of reactions and components. For a model including k reactions, n_f fluid components and n_s solid components, each reaction gives 3 additional groups plus $n_f + n_s$ stoichiometric coefficients (Table 9). Since $a_{i,i} = -1$ and $\sum_j a_{ij} = 0$, the number of independent stoichiometric coefficients for each reaction is $n_f + n_s - 2$. Each fluid component gives 8 additional groups (Table 12) and each solid component gives 2 additional groups (Table 13). The model also depends on 9 general heat and mass flow numbers (Table 7). Therefore, the total number of dimensionless numbers is equal to $9 + k(3 + n_f + n_s - 2) + 8n_f + 2n_s$.

For test case 1 which includes three reactions, five fluid components and one solid component, this amounts to 72 dimensionless numbers. For test case 2 which includes three reactions, four fluid components and two solid components, this amounts to 66 dimensionless numbers. A sensitivity analysis with DOE for such a large number of parameters would result in an impractical amount of computation.

To conduct this sensitivity analysis, we first restrict ourselves to a model with one reaction and four components. Then, we study the evolution of the production profile for test cases 1 and 2 when changing the Damköhler numbers, and finally we identify the optimal heater temperature for the process as a function of these Damköhler numbers.

We consider a simplified model with one reaction:

$$K \longrightarrow O + G + C \tag{19}$$

where K is the kerogen, O an oil component, G a gas component and C the solid charred residual. This chemical reaction gives five dimensionless groups ($D_K, Na, \Delta h_r^*, a_G$ and a_o). To simplify further the problem, we assume that the oil and gas components are immiscible. In this case, the component O gives four groups (ρ_O^*, c_O^*, e_O^* and γ_O^*) and the component G gives two groups (ρ_G^* and γ_G^*). The kerogen and solid residual each give two groups ($\rho_{s,j}^*$ and γ_j^*) but since K is the primary reactant, $\rho_{s,K}^* = 1$ and $\gamma_K^* = 1$. Therefore, this simplified model has 22 dimensionless groups. Their minimum and maximum values can be found in Table 17.

We used DOE to study (1) the production time and (2) the energy efficiency of the process. We applied a first order model with interactions and a two-level fractional factorial design of resolution 5 [14]. The design generates 512 simulations with different values of the dimensional groups.

We define the production time t_{prod} as the time it takes for the process to reach 99% of its total cumulated hydrocarbon mass recovery, and the dimensionless production time as the ratio between t_{prod} and τ. Fig. 3 shows a tornado chart of the 10 most important effects. The threshold value is obtained by comparison with the variance of the standard student distribution [14]. The interaction effects have been computed too and we observed that the most important ones are interactions between parameters with important effects. They have not been included in Fig. 3 since they do not bring any additional information.

The Damköhler number D_K is the most important number. The larger it is, the faster the chemical reactions and therefore the faster the process. The heat capacity ratio Γ is the second most important number. The larger it is, the longer it takes to bring the system to a large temperature. The reduced reaction enthalpy Δh_r^* also has a large impact. The larger it is, the more energy is consumed by the chemical reaction, leading to a delay in production. The other numbers have either a limited or insignificant impact.

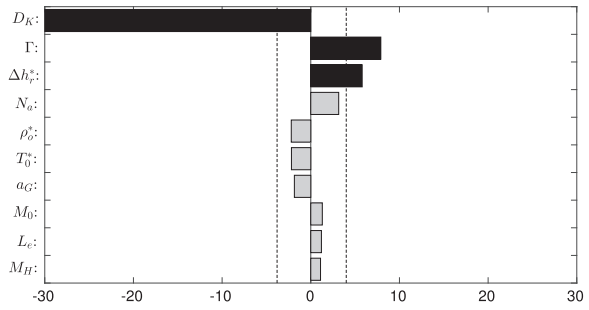

Fig. 3. Tornado chart of the 10 most important effects for dimensionless production time of simplified ISU model. The threshold value is obtained by comparison with the variance of the standard student distribution [14].

The next step is to define a measure of performance for the energy efficiency of the process. The final EROI of the process represents its thermodynamic efficiency. It increases as the temperature decreases but then so does the production time. To define the energy efficiency of the process, we need to define a target maximum production time. Fig. 4 shows the distribution of the production time during the factorial design experiment. We observe that 49.6% of the simulations reached their total production after a dimensionless time between 0 and 16τ, which means that more than 50% of the simulations have not reach their total production after a time equal 16τ. For test cases 1 and 2, 16τ is equal to 35 and 37 years, respectively, so it is not reasonable to wait that long. This happens when the heater temperature is too low to properly convert the kerogen into oil and gas. We also observe that more than 20% of the simulations are reaching their total production after a time of approximately 2τ. For test cases 1 and 2, 2τ is equal to 4.4 and 4.7 years, respectively, which is in the range of production time of 1–5 years expected for these processes [12,7]. Therefore, 2τ seems a reasonable target maximum production time. To evaluate the energy efficiency of the process, we then apply a production scenario where we stop the heating when the production stops or when we reach $t = 2\tau$, and we choose as a measure of performance the EROI obtained with this production scenario:

$$\text{Energyefficiency} = \text{EROI}\big(\min(t_{prod}, 2\tau)\big) \tag{20}$$

Fig. 5 shows a tornado chart of the 10 most important effects. Again, the interaction effects have not been included here as they do not bring additional information.

Again, the Damköhler number D_K is the most important number. The larger it is, the faster the chemical reactions and therefore the more efficient the process. The heat capacity ratio Γ is the second most important number. The larger it is, the more energy

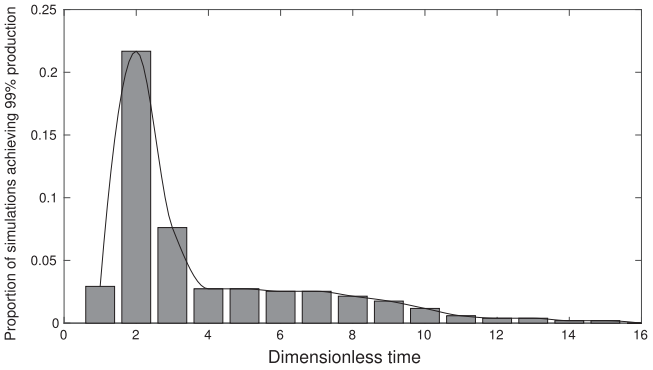

Fig. 4. Distribution of production time for 512 factorial design experiment [14]. The total grey area is equal to 0.496. The area in grey at $t_D = 2$ is equal to 0.217.

needed to bring the system to high temperature. The gas stoichiometric coefficient a_G and the reduced reaction enthalpy Δh_r^* also have a large impact. A larger a_G means that more gas is generated by chemical reactions, and as a result less coke. Therefore, the process is more efficient. The coefficient a_G has a larger impact than a_O since natural gas has a higher energy content that crude oil [42]. A larger Δh_r^* means that more energy is consumed by the chemical reactions and therefore the process is less efficient. The other numbers have either a limited or insignificant impact.

For both measures of performance, the Damköhler number D_K is the most important dimensionless number. This suggests that the most important coupling in the process is between the chemical reaction and the heat propagation, and that the oil and gas that is generated by the pyrolysis will simply flow to the well. Obviously, this might not be the case if the domain were not homogeneous in which case the fluid could get trapped inside the reservoir. Nevertheless, it is essential to evaluate it accurately.

6. Study of production profile

We observed earlier that using the Wellington et al. [35] kinetic model gave a Damköhler number for the decomposition of kerogen that is wrong by a factor of between 5 and 150. In the next section, we explore the effect of these errors on the production profile for test cases 1 and 2. Studying the impact of the Damköhler number on the energy efficiency and production time of the process in more details could give us new insights that can help identify better production scenarios.

Reaction enthalpies are generally ignored in previous works describing numerical simulation of the ISU process [12,39,23]. However, we observed in Section 5 that Δh_r^* is a primary number for both production time and energy efficiency. This suggests that evaluating the reaction enthalpy accurately is crucial for accurate simulation of the process. Therefore, we will also study the impact of reaction enthalpies for test case 1 and 2.

6.1. Variability of production profile with Damköhler numbers

For test cases 1 and 2, we have three Damköhler numbers, one for each reaction. We study the impact of getting these Damköhler numbers wrong by a factor of 100 on the production profile.

For test case 1, the values of the Damköhler numbers for the three reactions were initially $D_{K1} = 1540, D_{K2} = 470$ and $D_{K3} = 19$ (Table 10). Fig. 6 shows the hydrocarbon production profile (black line). Initially, we produce essentially liquid oil with low API°. As the temperature increases, the chemical reactions become important, the API° increases and we start producing gas. Since light oil and gas are more valuable products, the EROI of the process increases significantly (Fig. 6d). The production stops after a time of 1550 days, which corresponds to 1.98τ.

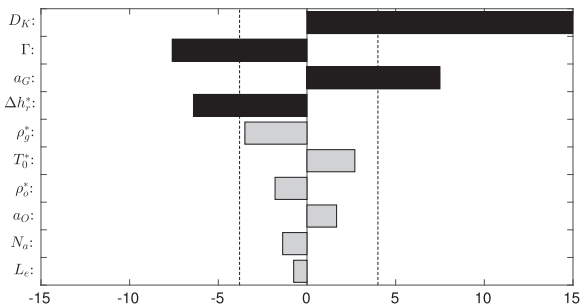

Fig. 5. Tornado chart of the 10 most important effects for EROI of simplified ISU model. The threshold value is obtained by comparison with the variance of the standard student distribution [14].

For test case 2, the values for the three reactions were initially $D_{K1} = 90, D_{K2} = 280$ and $D_{K3} = 34$ (Table 10). Fig. 7 shows the hydrocarbon production profile (black line). Initially, there is almost no production. As the temperature increases, the chemical reactions become significant and light components appear. The lighter components travel rapidly to the production well, so we start producing gas and light oil with API°≈ 45 (Fig. 7c). Later, some of the heavier hydrocarbon components reach the well and the API° decreases rapidly. Finally, as the last reaction appears, medium oil is converted to gas and the API° increases again. Since light oil and gas are more valuable products, the EROI of the process increases significantly (Fig. 7d). The production stops after a time of 1360 days, which corresponds to 1.64τ.

We then changed the values of the Damköhler numbers by multiplying the pre-exponential factors A_i by 100 or 0.01 for test cases 1 and 2. For test case 1, we observe that increasing the Damköhler numbers has two effects: (1) it accelerates the conversion, therefore reducing the production time and (2) it increases the production of gas and as a result increases the EROI. The production times are now 1030 days for test case 1, which corresponds to 1.3τ and 930 days for test case 2, which corresponds to 1.1τ. Accordingly, decreasing the Damköhler number increases the production time and decreases the EROI.

We observe that reducing the Damköhler number has a stronger impact on test case 2 than on test case 1. This is because for test case 1, the Damköhler number of the primary reaction $D_{K1} = 1540$ is larger than 1000. For $D_K = 1540$ or $D_K = 15.4$, the chemical reaction is fast compared to heat diffusion, and the time scale of the process is mostly limited by the heat diffusion time scale. However, for test case 2, the Damköhler number of the primary reaction $D_{K1} = 90$. When we divide this number by 100, the chemical reaction is no longer fast compared to heat diffusion.

To summarise, we observe that (1) evaluating the Damköhler numbers accurately is crucial to obtain the right production profile and (2) to obtain the best EROI with a production time lower than 2τ, we need a large D_{K1}, at least larger than 10.

6.2. Variability of the production profile with reaction enthalpies

Next, we consider the impact of the reduced reaction enthalpies. Initially, they were neglected. To observe their impact on the production profile for test cases 1 and 2, we successively change them from 0.0 to the values defined in Table 11. Figs. 8 and 9 show the variation of production profile for both test cases.

For test case 1, including the reaction enthalpy for the NSO decomposition ($\Delta h_{r1}^* = 0.56$) slows down the production of light oil and gas as the chemical reaction requires more energy to progress. The energy efficiency of the process is reduced and the production time increases to 1730 days, which corresponds to 2.2τ. Including the reaction enthalpy for the heavy oil decomposition ($\Delta h_{r2}^* = 0.31$) slows down the production of light oil and gas. The EROI is slighty reduced and the production time is further increased to 1840 days, which corresponds to 2.35τ. Finally, including the reaction enthalpy for the medium oil decomposition ($\Delta h_{r3}^* = 1.7$) has only a small impact as it only affects the end part of the profile. The final production time is 1910 days, which corresponds to 2.44τ.

For test case 2, the reaction enthalpy of the primary reaction (decomposition of K) is small ($\Delta h_{r1}^* = 0.1$), so only has a small impact on the production profile. the production time increases to 1390 days, which corresponds to 1.67τ. The reaction enthalpies

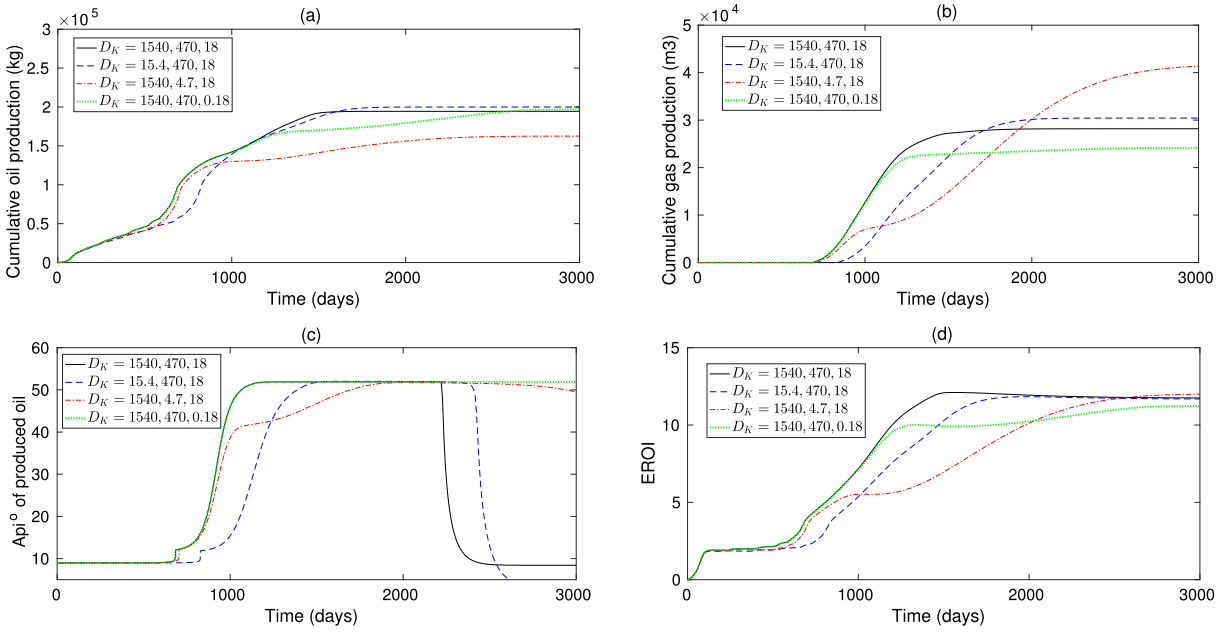

Fig. 6. Variation of hydrocarbon production profile with Damköhler numbers for test case 1.

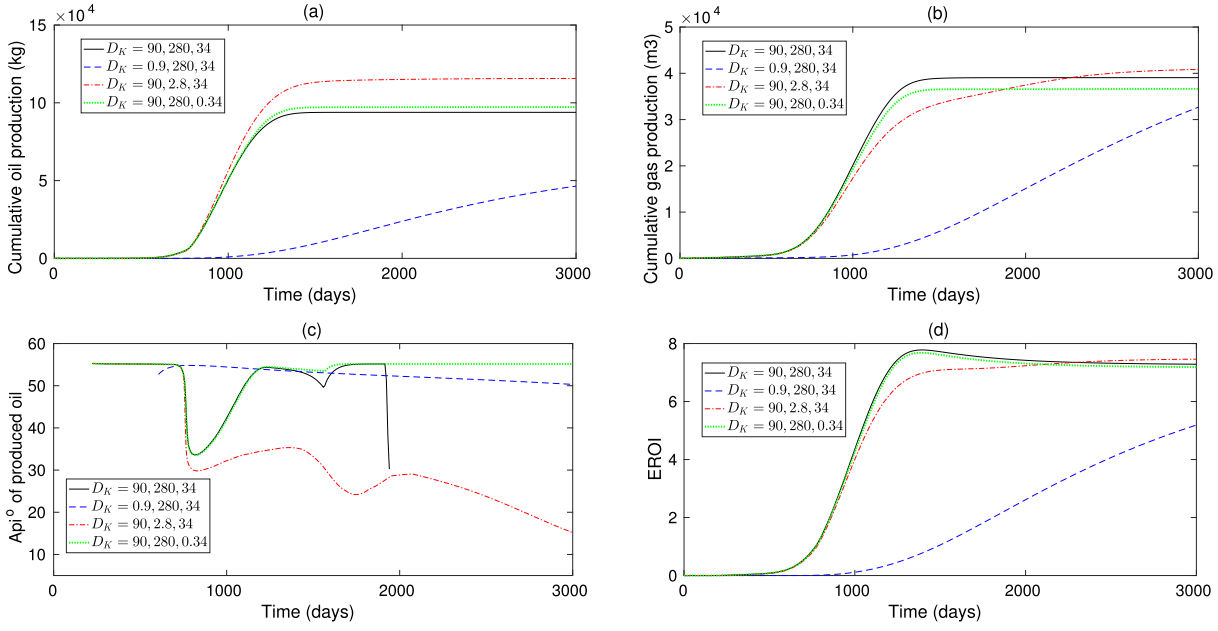

Fig. 7. Variation of hydrocarbon production profile with Damköhler numbers for test case 2.

for the heavy component is larger $(\Delta h^*_{r2} = 0.51)$, however since $D_{K2} > D_{K1}$, the reaction constant is already large when the reactant IC_{37} appears. The energy barrier is rapidly overcome and the reaction enthalpy has only a small impact. The production time further increases to 1460 days, which corresponds to 1.75τ. Finally, the reaction enthalpy for the medium oil decomposition $(\Delta h^*_{r3} = 2.5)$ again only has a small impact as it only affects the end part of the profile.

So we observe that the impact of reaction enthalpies can be important, especially for the first two reactions. Since reaction enthalpies represent additional energy that needs to be given to the system, including them results in retarding the production. This in turn reduces the EROI. Therefore, they should not be neglected, but measured accurately.

6.3. Identification of optimal heater temperature

The Damköhler numbers are not independent as they describe chemical reactions of the same kinetic model and they all depend on the temperature of the heaters. Generally, D_{K3} is smaller than D_{K1} and D_{K2} as it describes the decomposition of a lighter component.

These Damköhler numbers depend on two parameters that are controlled by the operator: the distance between two heaters and the heater temperatures. The distance between heaters should be as small as possible, so to heat up the reservoir as fast and as uniformly as possible, and therefore reduce the production time. The minimum distance between heaters will then be determined by economics and engineering considerations [5].

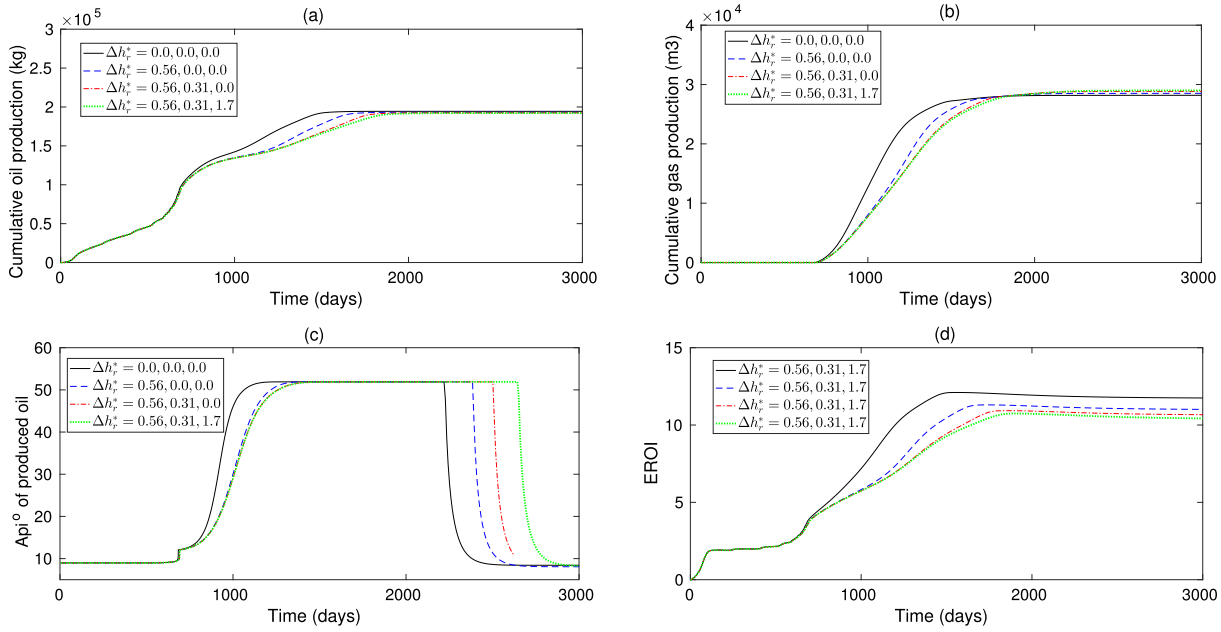

Fig. 8. Variation of hydrocarbon production profile with reduced reaction enthalpies for test case 1.

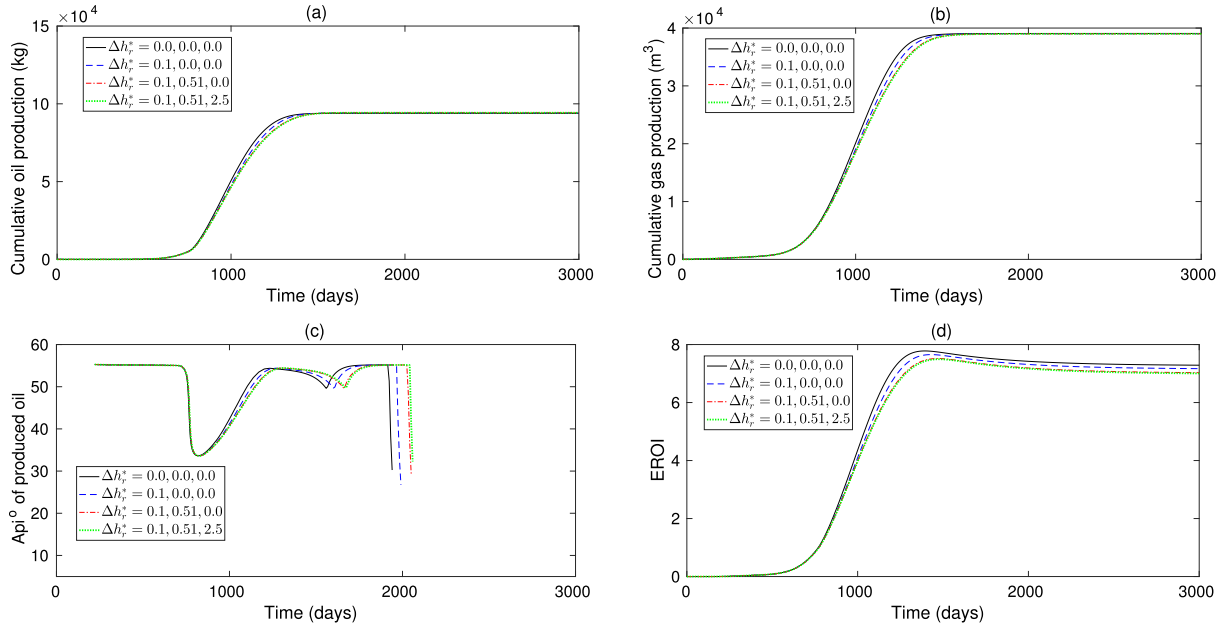

Fig. 9. Variation of hydrocarbon production profile with reduced reaction enthalpies for test case 2.

A large temperature is crucial for the conversion of kerogen and bitumen, but setting the heater temperature as large as possible may not be necessary. Indeed, a Damköhler number of 100 or 1000 makes little difference for the production time since it would then be mostly restricted by the time scale of the thermal diffusion. Moreover, at very large Damköhler numbers, most reactant is converted before we reach the heater temperature, and the additional energy is then used to simply heat up the rock. These considerations suggest the existence of an optimal heater temperature for the energy efficiency of the process (Eq. (20)).

In this section we study the impact of the heater temperature on the production time and energy efficiency of the process. We perform numerical simulations with the heater temperature varying from 250 °C to 400 °C for test cases 1 and 2. Fig. 10 shows the evolution of the dimensionless production time. For both test cases, it is larger than 20 for $T_H = 250$ °C. At $T_H = 300$ °C, it is equal to 8.9 for test case 1 and 3.5 for test case 2. At $T_H = 350$ °C, the dimensionless production time is equal to 1.98 for test case 1 and 1.7 for test case 2. Finally, at $T_H = 400$ °C, it is equal to 1.25 for both test cases.

We observe that the production time decreases rapidly when we increase the temperature from $T_H = 250$ °C until we reach a production time of around 2.0τ, at $T_H = 345$ °C for test case 1 and $T_H = 331.5°$ for test case 2. At these temperatures, the Damköhler numbers are $D_{K1} = 1110, D_{K2} = 313$ and $D_{K3} = 12$ for test case 1 and $D_{K1} = 34.7, D_{K2} = 84.5$ and $D_{K3} = 9.5$ for test case 2. This confirms the result of our sensitivity analysis and validates the choice of 2τ as our target production time. The production time

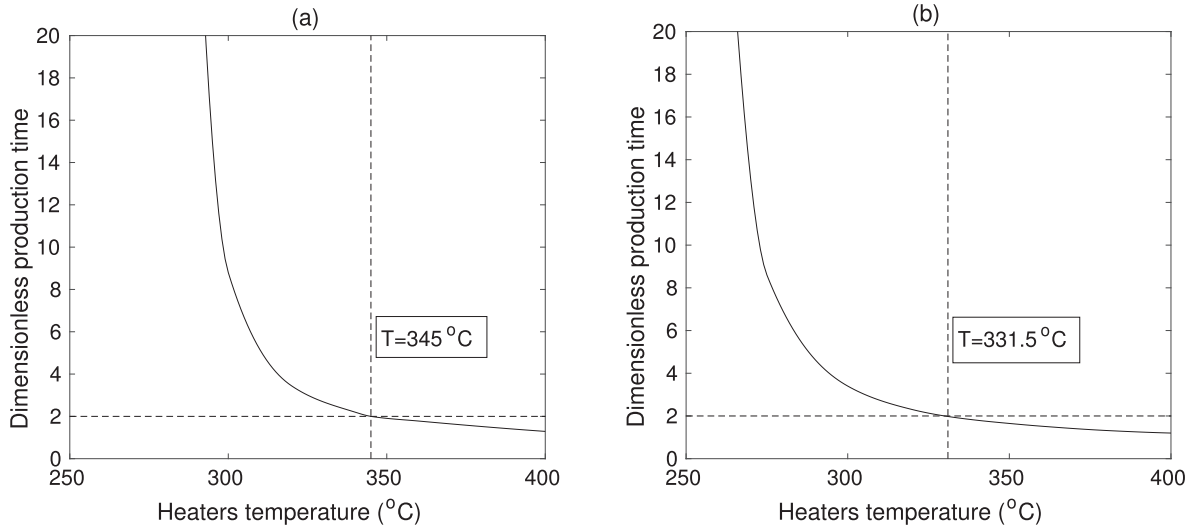

Fig. 10. Evolution of dimensionless production time with heater temperature for (a) test case 1 and (b) test case 2. The production time decreases rapidly when we increase the temperature from $T_H = 250$ °C until we reach a production time of around 2.0τ at $T_H = 345$ °C for test case 1 and $T_H = 331.5°$ for test case 2.

continues to decrease for higher temperature, but more slowly, remaining larger than τ. With significantly more energy spent in the process, it might not be interesting to keep increasing the heater temperature. Fig. 10 shows the evolution of the EROI for a production scenario where we stop the process when the production stops or when $t = 2\tau$ for test cases 1 and 2 (Eq. (20)). We observe for both case an optimal heater temperature.

When the heater temperature is low, the chemical reactions are too slow for the process to be efficient. When the heater temperature is very large, the decomposition is completed before the domain reaches the maximum temperature and a significant part of the energy invested is used to simply heat up the rock.

Fig. 11a shows a maximum EROI for a temperature of 346.5 °C and Fig. 11b shows a maximum EROI for a temperature of 333 °C. At these temperatures, the Damköhler numbers are $D_{K1} = 1230, D_{K2} = 354$ and $D_{K3} = 13.8$ for test case 1 and $D_{K1} = 37.5, D_{K2} = 93.6$ and $D_{K3} = 10.5$ for test case 2. We observe that for both test cases, the optimal energy efficiency is obtained when the lowest of the Damköhler numbers of the set of reactions included in the model is between 10 and 20. We conclude that the optimal temperature of the process for a model with k reactions lies within the range:

$$\max_{1\leqslant i\leqslant k} T_{R=10,i} \leqslant T_{opt} \leqslant \max_{1\leqslant i\leqslant k} T_{R=20,i} \tag{21}$$

where $T_{R=\lambda,i}$ is the temperature for which the dimensionless rate of reaction i is equal to λ:

$$T_{R=\lambda,i} = \frac{E_{ai}}{R\log(D_{Ki}/\lambda)} \tag{22}$$

Eq. (21) has been obtained for a cubic geometry with four heaters, one on each vertical side of the cube. However, since the heater pattern mainly impacts the time taken to bring the formation to a high temperature, the result should hold as long as the characteristic length L of the domain is correctly defined.

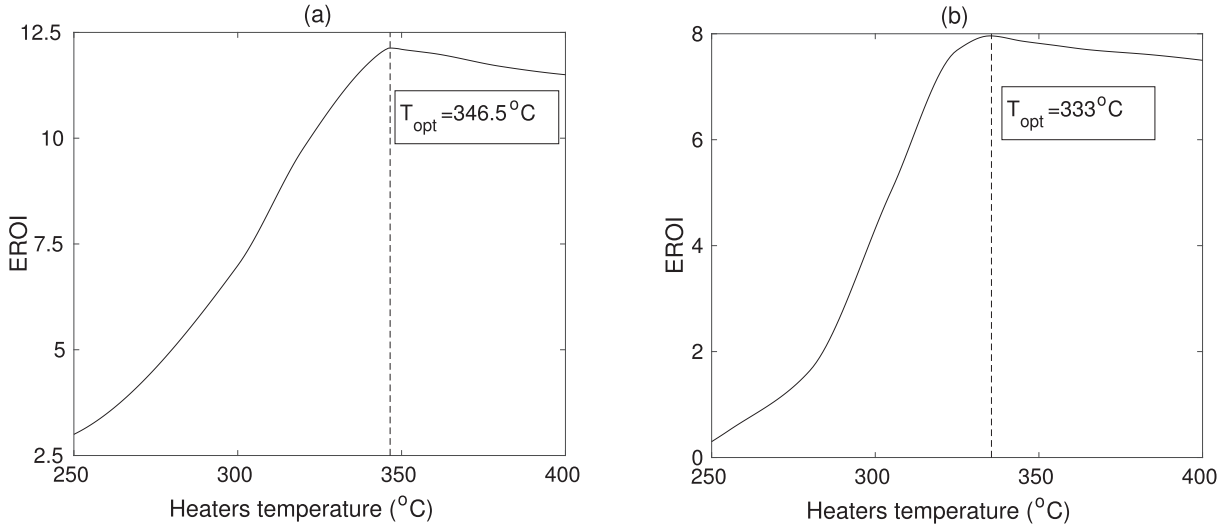

Fig. 11. Evolution of EROI with heater temperature for (a) test case 1 and (b) test case 2. We stop the process when the production stops or when $t = 2\tau$. When the heater temperature is low, the chemical reactions are too slow and the process is not efficient. When the temperature is very large, the decomposition is completed before the domain reaches the maximum temperature and a significant part of the energy invested is used to simply heat up the rock. The optimal temperature is obtained at $T = 346.5$ °C for test case 1 and $T = 333$ °C for test case 2.

This correlation can be used to reduce the number of numerical experiments necessary to identify the optimal production scheme. For test case 1, $T_{R=10} = 343\,^{\circ}\text{C}$ and $T_{R=20} = 351\,^{\circ}\text{C}$. Therefore, we know before performing any numerical simulation that the optimal temperature is somewhere in the interval [343 °C 351 °C]. For test case 2, the corresponding interval is [332 °C 342 °C].

Now, if the heater temperature is fixed, for example to 350 °C, Eq. (21) gives a characteristic length interval. For test case 1, $T_{R=10} = 350\,^{\circ}\text{C}$ corresponds to $L = 7.3$ m and $T_{R=20} = 350\,^{\circ}\text{C}$ corresponds to $L = 10.4$ m, so the optimal characteristic length is somewhere in the interval [7.3 m 10.4 m]. For test case 1, $T_{R=10} = 350\,^{\circ}\text{C}$ corresponds to $L = 5.4m$ and $T_{R=20} = 350\,^{\circ}\text{C}$ corresponds to $L = 7.6$ m, so the optimal characteristic length is somewhere in the interval [5.4 m 7.6 m].

7. Conclusion

This work has focused on the scaling analysis of the In-Situ Upgrading (ISU) process in order to identify the most important parameters for the energy efficiency of the process. For this, we developed a mathematical model that can describe the ISU of both heavy oil and bitumen and we demonstrated that for a model with n_f fluid components (gas and oil), n_s solid components and k chemical reactions, the process can be represented by $9 + k \times (3 + n_f + n_s - 2) + 8n_f + 2n_s$ dimensionless numbers. They were calculated for two test cases, one describing the ISU of Athabasca bitumen, and one describing the ISU of oil shale, and a range of values for each dimensionless number was obtained from a thorough literature review. Then, we performed a sensitivity analysis using Design of Experiment (DOE) and Response Surface Methodology (RSM) to identify the primary parameters controlling the production time and energy efficiency of the process.

For each reaction, the Damköhler number D_K quantifies the ratio of chemical rate to heat conduction rate at the specified heater temperature. It describes how fast the chemical reaction is compared to the thermal diffusion time scale τ, at that heater temperature. The sensitivity analysis showed that D_K is the most important parameter controlling the production time. To define the energy efficiency of the process, we observed that more than 50% of the simulations have not reach their total production after a time equal 16τ and that more than 20% of the simulations reach their total production after a time of approximately 2τ. Therefore, we chose as a measure of performance of the energy efficiency of the process the EROI at a time equal to the minimum of t_{prod} and 2τ (Eq. (20)). Again, we observed that the Damköhler number is the primary parameter controlling the efficiency of the process.

The Damköhler number depends mostly on the activation energy of the reaction. Therefore, it is essential to measure the activation energy of the reactions accurately. For test case 2, we used activation energies and pre-exponential factors from Wellington et al.'s kinetic model [35] and obtained an uncharacteristically low Damköhler number for the kerogen decomposition. For this model, activation energies and pressure-dependent pre-exponential factors were experimentally determined over a range of temperatures from 0 to 300 °C. On the contrary, Braun and Burnham [31] present activation energies and pre-exponential factor that have been experimentally validated over a wider range of temperatures from 0 to 600 °C. They propose a kinetic model where each decomposition is modelled by several reactions. Each one of these reactions concerns a certain fraction of the reactant and uses its own activation energy. This way, the decompositions are described more accurately over a wider range of temperatures. Behar et al. [13] proposed a similar kinetic model for the decomposition of bitumen. To describe accurately the chemical reactions, we recommend using a model similar to these.

We also found that the reduced reaction enthalpies were important parameters and should be evaluated accurately. We showed that for the test case 1, using the bitumen reaction enthalpies from Phillips et al. [18] will impact significantly the production profile.

Further analysis showed that for test cases 1 and 2, the process is most efficient for Damköhler numbers larger than 10. In this case, the production time is lower than 2τ. When the heater temperature was low, the Damköhler numbers were too small and the chemical reactions too slow. The production time decreases rapidly when we increase the temperature until we reach a production time of around 2τ. The production time continues to decrease for higher temperatures, but more slowly, remaining larger than τ. However, when the heater temperature was very high, the decomposition was completed before the domain reaches the maximum temperature and an important part of the energy invested was used to simply heat up the rock. Therefore, the production time of the process can be further reduced by increasing the temperature, but this is done at the expense of the process energy efficiency. Our analysis shows that imposing a higher temperature and stopping heating when no more oil is produced does not give a larger EROI. We observed that for both test cases, the optimal energy efficiency was obtained when the minimal Damköhler number was between 10 and 20. This correlation can be used to define an interval in which to search for an optimal heater temperature (if the reference length is defined) or an interval in which to search for an optimal reference length (if the heater temperature is defined). This could reduce significantly the numbers of numerical simulations that need to be performed to identify the best production scenario.

However, our analysis has six limitations that should be noted:

1. Component lumping and experimental correlations for phase equilibrium and phase properties are used instead of more accurate equations of state. A more precise compositional and chemical model should be used to model the process more accurately.
2. Water has not been included, since in ISU, the reactions of interest occur mostly above the boiling point of water. Nevertheless, the impact of water-filled pores should be investigated in future work, since the enthalpy of evapouration and vapour volume could be significant.
3. Heat loss has been neglected. Fan et al. [12] demonstrated that heat loss to overburden and underburden could have an impact on the efficiency of the process depending on the ratio of formation thickness to well spacing. The wider the well spacing and the thinner the formation then the more important heat loss becomes.
4. Since all numerical simulation have been performed with an $11 \times 11 \times 1$ grid, the effect of gravity has been effectively neglected. The importance of gravity can be quantified by the gravity number:

$$N_g = \frac{\Delta\rho g D L}{\Delta P} \tag{23}$$

   For test cases 1 and 2, the pressure build up in the reservoir is approximatively 30 bars, which gives a gravity number of approximatively 0.3. This suggests that gravity is not dominant, but should be included in future work to increase accuracy.
5. Heat capacity and thermal conductivity have been assumed constant. They can vary significantly with temperature from initial to heater condition.
6. The permeability only changes with the solid phase saturation. For domains with low permeability such as oil shale, the pressure rise in the domain can lead to the formation of fractures [38]. To describe the ISU of oil shale more accurately, our model needs to include these fractures, and so needs to be coupled

with a geomechanical model for fracture propagation. Future work could investigate whether the correlation for optimal energy efficiency still holds when these additional effects are included.

Moreover, the choice of 2τ as our target maximum production time for the energy efficiency of the process (Eq. (20)) has been obtained based on the outcomes of the simulations performed for the sensitivity analysis in combination with an assessment of practical production timescales for real field implementations. Additional parameters such as heating management, return on capital or human patience can greatly affect this target maximum production time. In this case, the same analysis should be reproduced to assess if the Damköhler number is still the primary parameter and if the optimal temperature still lies in the same interval.

Finally, we note that numerical simulations of the ISU process using an accurate kinetic model such as the ones defined in Braun and Burnham [31] or Behar et al. [13] generally takes a lot of computational time. These models include a large number of components (>20) to describe accurately the chemical rates. Operator Splitting (OS) methods [43] could be applied in order to deal separately with the transport and chemical reaction parts, and use a small amount of lumped component for the transport part. The use of OS methods has been investigated for 1D ISU problems [17]. Future work could focus on extending the results to a more complete 3D models and use OS as the basis of an algorithm to reduce the computational time with minimum loss in accuracy.

Acknowledgement

The authors are grateful to Total E&P for sponsoring this work.

References

[1] Meyer RF, Attanasi ED, Freeman P. Heavy oil and natural bitumen resources in geological basins of the world. US geological survey open-file report 2007-1084.
[2] Butler RM, Stephens DJ. The gravity drainage of steam-heated heavy oil to parallel horizontal wells. J Can Petrol 1991;20(2):90–6.
[3] Siu AL, Nghiem LX. Modelling steam assisted gravity drainage process in the UTF. In: SPE annual technical conference and exhibition, Dallas, Texas, USA, 6–9 October.
[4] Butler RM. SAGD comes to age! J Can Petrol Technol 1998;37(7):9–12.
[5] Fowler T, Vinegar H. Oil shale ICP-Colorado field pilot. In: SPE Western regional meeting, San Jose, California, USA, 24–26 March 2009.
[6] Kumar J, Fusetti L, Corre B. Modeling in-situ upgrading of extraheavy oils/tar sands by subsurface pyrolysis. In: Canadian unconventional resources conference, Alberta, Canada, 15–17 November 2011.
[7] Snow R. In-situ upgrading of bitumen and shale oil by RF electrical heating. In: SPE heavy oil conference and exhibition, Kuwait City, Kuwait, 12–14 December.
[8] Tissot B, Welte DH. Petroleum formation and occurence. 2nd ed. Berlin (Germany): Springer-Verlag; 1984.
[9] Behar F, Lorant F, Lewan M. Role of NSO compounds during primary cracking of a type II kerogene and a type III lignite. Org Geochem 2008;39:1–22.
[10] Alpak FO, Vink JC. Adaptive local-global multiscale simulation of the in-situ conversion process. SPE J 2016;21(06):2112–27.
[11] Braun RL, Burnham AK. Mathematical model of oil generation, degradation, and expulsion. Energy Fuels 1990;4(2):132–46.
[12] Fan Y, Durlofsky L, Tchelepi H. Numerical simulation of the in-situ upgrading of oil shale. SPE J 2010;15(2):368–81.
[13] Behar F, Lorant F, Mazeas L. Elaboration of a new compositional kinetic schema for oil cracking. Org Geochem 2008;39:764–82.
[14] Myers RH, Montgomery DC, Anderson-Cook CM. Response surface methodology: process and product optimization using design of experiments. 3rd ed. Oxford: John Wiley and Sons Inc.; 2009.
[15] Ruzicka MC. On dimensionless numbers. Chem Eng Res Des 2008;86(8a):835–68.
[16] Shook M, Li D, Lake WL. Scaling immiscible flow through permeable media by inspectional analysis. IN SITU 1992;16(4):311–49.
[17] Maes J, Muggeridge AH, Jackson MD, Quintard M, Lapene A. Modelling in-situ upgrading of heavy oil with operator splitting method. J Comput Geosci 2016;20(3):581–93.
[18] Phillips C, Luymes R, Halahel T. Enthalpies of pyrolysis and oxidation of Athabasca oil sands. FUEL 1981;61:639–46.
[19] Camp D. Oil shale heat capacity relations and heat of pyrolysis and dehydration. In: 20th Oil shale symposium.
[20] Gersten J, Fainberg V, Hetsroni G, Shindler Y. Kinetic study of the thermal decomposition of polypropylene, oil shale, and their mixture. FUEL 1999;79(13):1679–86.
[21] Watts JW. A compositional formulation of the pressure and saturation equations. SPE Reserv Eng 1986;1(3):243–53.
[22] Corey AT. The interrelation between gas and oil relative permeabilities. Producers Mon 1954;19(1):38–41.
[23] Lee K, Moridis GJ, Ehlig-Economides CA. A comprehensive simulation model of kerogen pyrolysis for the in-situ upgrading of oil shales. In: SPE reservoir simulations symposium, Houston, Texas, USA, 23–25 February.
[24] Li H, Vink JC, Alpak FO. An efficient multiscale method for the simulation of in-situ conversion processes. SPE J 2015;20(3):579–93.
[25] Wilson G. A modified Redlich-Kwong EOS, application to general physical data calculations. In: Annual AIChE national meeting, Cleveland, Ohio, USA, 4–7 May.
[26] Mifflin RT, Watts JW, Weiser A, Rice U. A fully coupled, fully implicit reservoir simulator for thermal and other complex reservoir processes. In: SPE symposium on reservoir simulation, Anaheim, California, USA, 17–20 February.
[27] Young LC, Stephenson RE. A generalized compositional approach for reservoir simulation. SPE J 1983;23(5):727–42.
[28] Ashrafi M, Souraki Y, Karimaie H, Torsaeter O, Bjorkvik BJA. Experimental PVT property analyses for Athabasca bitumen. In: Canadian unconventional resources conference, Alberta, Canada, 15–17 November.
[29] CMG-STARS. User's guide. Computer Modeling Group Ltd; 2012.
[30] Al Darouich T, Behar F, Largeau C. Thermal cracking of the light aromatic fraction of Safaniya crude oil: experimental study and compositional modelling of molecular classes. Org Geochem 2006;37:1130–54.
[31] Braun RL, Burnham AK. PMOD: a flexible model of oil and gas generation, cracking, and expulsion. Adv Org Geochem 1992;19(1–3):161–72.
[32] Freund H, Clouse JA, Otten GA. The effect of pressure on the kinetics of kerogen pyrolysis. Energy Fuels 1993;7(6):1088–94.
[33] Savage PE, Klein MT. Asphaltene reaction pathways.2. Pyrolysis of n-pentadecyclbenzene. Ind Eng Chem Res 1987;26:488–94.
[34] Miadonye A, Singh B, Puttagunta VR. Modeling the viscosity-temperature relationship of Alberta bitumens. Fuel Sci Tech Int 1994;12(2):335–50.
[35] Wellington SL, Berchenko IE, Rouffgnac EP, Fowler TD, Ryan RC, Shahlin GT, et al. In situ thermal processing of an oil shale formation to produce a desired product. US Patent No. 6880633.
[36] Gharbi RBC. Dimensionally scaled miscible displacements in heterogeneous permeable media. Transp Porous Media 2002;48(3):271–90.
[37] Maes J, Muggeridge AH, Jackson MD, Quintard M, Lapene A. Scaling heat and mass transfer in the presence of pyrolysis. Heat Mass Transf (Wärme Stoffübertrag) 2014;51(3):331–4.
[38] Kobchenko M, Panahi H, Renard F, Dysthe DK, Malthe-Sorenssen A, Mazzini A, et al. 4D imaging of fracturing in organic-rich shales during heating. J Geophys Res 2001;116.
[39] Lee K, Moridis GJ, Ehlig-Economides CA. Oil shale in-situ upgrading by steam flowing in vertical hydraulic fractures. In: SPE unconventional resources conference, The Woodlands, Texas, USA, 1–3 April.
[40] Wen CS, Yen TF. A comparison between the properties of devonian shale and green river oil shale via thermal analysis. Advances in Chemistry 1979;183(20):343–51.
[41] Li P, Chalaturnyk RJ. History match of the UTF phase. A project with coupled reservoir geomechanical simulation. J Can Petrol Technol 2009;48(1):29–35.
[42] Perry RH, Green DW. Perry's chemical engineering handbook. 6th ed. McGraw Hill; 1984.
[43] Holden H, Karlsen KH, Lie K, Risebro N. Splitting methods for partial differential equations on rough solutions. European Mathematical Society; 2010.